Journal of Alloys and Compounds 851 (2021) 156793

Contents lists available at ScienceDirect

Journal of Alloys and Compounds

journal homepage: http://www.elsevier.com/locate/jalcom

A high conductive TiC–TiO_2/SWCNT/S composite with effective polysulfides adsorption for high performance Li–S batteries

Xianwei Geng [a, b], Ruowei Yi [c, d], Xiangfei Lin [d], Chenguang Liu [a, b], Yi Sun [a, b], Yingchao Zhao [a, b], Yinqing Li [e], Ivona Mitrovic [a, f], Rui Liu [g], Li Yang [d, **], Cezhou Zhao [b, *]

[a] Department of Electrical Engineering and Electronics, University of Liverpool, Liverpool, L69 3GJ, United Kingdom
[b] Department of Electrical and Electronic Engineering, Xi'an Jiaotong-Liverpool University, Suzhou, 215123, China
[c] Stephenson Institute for Renewable Energy, Department of Chemistry, University of Liverpool, Liverpool, L69 7ZD, United Kingdom
[d] Department of Chemistry, Xi'an Jiaotong-Liverpool University, Suzhou, Jiangsu, 215123, China
[e] Dongguan Hongde Battery Ltd.Co., Dongguan, 523649, China
[f] Centre for Advanced Materials, University of Liverpool, L69 3GH, United Kingdom
[g] National Demonstration Center for Experimental Materials Science and Engineering Education, Jiangsu University of Science and Technology, Zhenjiang, 212003, China

ARTICLE INFO

Article history:
Received 8 February 2020
Received in revised form
21 July 2020
Accepted 18 August 2020
Available online 20 August 2020

Keywords:
Lithium-sulfur batteries
Titanium carbide
Titanium dioxide
Single-walled carbon nanotube

ABSTRACT

Lithium-sulfur (Li–S) batteries have attracted more and more attention in recent years, as their theoretical capacity is several times larger than conventional lithium-ion batteries and they have a high energy density in secondary battery systems. In our work, a titanium carbide - titanium dioxide/single-walled carbon nanotube/sulfur (TiC–TiO_2/SWCNT/S) cathode with high conductivity and effective polysulfides adsorption is prepared by a facile method for fabricating Li–S batteries. The batteries with this composite cathode show a good performance at 0.1 C due to relatively high utilization of sulfur, reaching 1338.6 mAh·g^{-1} specific capacity at first cycle and retaining 802.5 mAh·g^{-1} after 100 cycles. Meanwhile, it presents an excellent rate performance with 711.2 mAh·g^{-1} at 4 C, and recovers to 1006.9 mAh·g^{-1} when the current returns to 0.1 C. Also a slow capacity decay (0.045% decay rate per cycle) is observed at 1 C. These results suggest that a small amount of SWCNT can increase the conductivity of the whole composite to a great extent, and the strong adsorption ability of TiO_2 increases the cycle life. This work offers an efficient and low-cost strategy to obtain high performance batteries with great potential for commercial applications.

1. Introduction

Driven by insufficient specific capacity of traditional lithium-ion batteries (<300 mAh·g^{-1}) for increasing demands today [1–3], the importance of lithium-sulfur (Li–S) batteries has been recognized as a promising next-generation energy applied to electric vehicles and other systems. Attractively high theoretical energy density of 2600 Wh·kg^{-1} and specific capacity of 1675 mAh·g^{-1}, moreover, abundant source of elemental sulfur in nature and nontoxicity advantage have stimulated many advanced developments in Li–S batteries [4,5]. However, several unresolved problems in Li–S batteries limit its applications as energy storage devices, and it is still a long way to go for commercial applications. These challenges are addressed as follows: Firstly, non-conductive nature of elemental sulfur (25 °C, 5 × 10^{-30} S·cm^{-1}) and lithium sulfides produced during the discharge process result in the low utilization rate of sulfur and poor rate performance [6]. Secondly, the volume of sulfur will expand about 80% when the discharge is completed, leading to the damage of the electrode and thus rapid capacity fading [7]. Thirdly, the dissolution and "shuttle effect" of polysulfides directly cause the self-discharge of the battery within hours and the loss of the active materials [8–10], consequently a fast decay of capacity [11,12].

In order to solve these issues, various methods have been dedicated and the main focus is to fabricate novel nanostructured composite cathodes. One of the popular choices is carbon material since it exists widely in nature and offers great conductivity, high

* Corresponding author.
** Corresponding author.
E-mail addresses: li.yang@xjtlu.edu.cn (L. Yang), cezhou.zhao@xjtlu.edu.cn (C. Zhao).

https://doi.org/10.1016/j.jallcom.2020.156793
0925-8388/

porosity and surface area. Moreover, carbon has flexible layered structure, which could wrap small-size active sulfur and effectively reduce the loss of sulfur [13]. The carbon-sulfur composites, such as graphene-sulfur [14,15], carbon nanotubes-sulfur [16–19], porous and hollow carbon spheres-sulfur, have become the most promising electrode materials benefited from a simple preparation process and superior improved capacity performance [20–23].

Another research hotspot is metal oxides that typically contain an anion (O^{2-}) with a strong polar surface [24]. Different from nanostructured carbon materials, nanostructured metal oxides afford abundant polar active sites to favor the absorption of polysulfides, facilitating the Li–S batteries with high sulfur utilization and long life span [25–29]. One good example was reported in Mingpeng Yu's work. They applied atomic layer deposition of titanium dioxide (TiO_2) layers on nitrogen-doped graphene/sulfur (NG/S) electrodes to avoid the capacity deterioration. It delivered initial discharge capacity up to 1069.5 mA $h \cdot g^{-1}$ and 918.3 $mAh \cdot g^{-1}$ after 500 cycles at 1 C [30]. Similarly, Xiao Liang's group applied S/vanadium pentoxide (V_2O_5)-graphene composite to obtain a decay rate of 0.048% per cycle at 0.05 C and Xiulei Ji's group employed a porous silicon dioxide (SiO_2) embedded within the carbon-sulfur composite to assist the absorption of polysulfides [31,32]. Most of the metal oxides, however, have poor conductivity and thus the slow electron transfer speed, which is unfavorable to the utilization of sulfur under the large current density. Hence, a challenge has been to develop a composite that can not only capture polysulfides but also enhance the conductivity of cathode.

In this work, we demonstrated a facile process to fabricate the titanium carbide - titanium dioxide/single-walled carbon nanotube/sulfur composite (TiC–TiO_2/SWCNT/S) to address this challenge. At the beginning, a simple oxidation reaction was carried out for turning TiC to TiC–TiO_2 composite. Then, SWCNT was mixed with TiC–TiO_2 through an ultrasonic dispersion technique to form the TiC–TiO_2/SWCNT composite. Finally, sulfur was deposited on the TiC–TiO_2/SWCNT composite by a melting-diffusion method and the final composite TiC–TiO_2/SWCNT/S was produced. Compared with previous work [33,34], TiC–TiO_2/SWCNT/S presents a higher capacity in large current density (850.7 $mAh \cdot g^{-1}$ at 1 C for the first cycle) and has a better rate performance (711.2 $mAh \cdot g^{-1}$ at 4 C) with improved conductivity. Another attractive feature is less conductive agent (super p) used during the slurry preparation process compared to previous study [33,34]. We improved the conductivity by modifying the composite materials with less conductive agent, namely the mass ratio of the composite: conductive agent: binder is now 8:1:1 rather than the previous reported one 7:2:1 [33,34]. This strategy is more cost effective and excellent performance with application potential achieved by increasing the energy density for the whole battery.

2. Experiment details

2.1. Chemicals and materials

Titanium carbide (≥99.9%, metals basis), titanium dioxide (≥99.8%, metals basis) and SWCNT (≥95%) were purchased from Aladdin Industrial Ltd. Co. Ethanol (≥99.8%) was purchased from Sinopharm Chemical Reagent Co. Ltd. Nitric acid (65.0–68.0%) was purchased from Jiangsu Qiangsheng Functional Chemistry Co. Ltd. Sulfur sublimed (≥99.5%) was purchased from Chengdu Kelong Chemical Reagent factory. The deionized (DI) water produced from a PURELAB (ELGA, UK) was used throughout for all the experiments.

2.2. Synthesis of TiC–TiO_2 composite

The TiC–TiO_2 composite was synthesized by a simple oxidation reaction. At first, 30 mL nitric acid (7 M) and 60 mL ethanol were mixed together and stirred for 5 min. Then, 600 mg TiC was added into the mixed solvent, stirred well and under ultrasonic dispersion for 10 min. Next, the mixture suspension was under magnetically stirred at 60 °C for 12 h. Finally, the suspension was centrifuged, washed with ethanol and DI water for several times. After dried at 80 °C by vacuum drying oven, the TiC–TiO_2 composite was obtained [35].

2.3. Synthesis of TiC–TiO_2/S and TiC–TiO_2/SWCNT/S composite

For both composites, sulfur loading was achieved through a melting-diffusion method. At the beginning, sublimed sulfur was mixed into TiC–TiO_2 composite with 3:1 ratio by weight, and then under ball-milling for 10 min in order to mix uniformly and ensure good homogeneity before the process of melting sulfur. The following procedure was applied for melting sulfur in the composites. Firstly, the powder was placed in a porcelain boat and transferred to a quartz tube, then heated at 155 °C for 10 h under the protection of Ar in the furnace. Next, the powder was heated to 200 °C in Ar and kept for 15 min to remove the excess sulfur on the surface. After cooling naturally to room temperature, the resultant composite was denoted as TiC–TiO_2/S [33].

For TiC–TiO_2/SWCNT/S composite, 15 wt%, 10 wt% and 5 wt% SWCNT (relative to the mass ratio of TiC) were mixed with TiC–TiO_2 respectively in ethanol via ultrasonic dispersion for 30 min. The suspension was then filtered and dried to obtain the TiC–TiO_2/SWCNT composite. These prepared composites and sublimed sulfur (TiC–TiO_2: S = 1:3 ratio by weight) were placed under the same ball-milling mentioned above. The melting sulfur procedure was the same as above, except the addition of SWCNT. The final products were named as TiC–TiO_2/SWCNT/S 15, TiC–TiO_2/SWCNT/S 10 and TiC–TiO_2/SWCNT/S 5, respectively. The schematic of the procedure for preparing TiC–TiO_2/SWCNT/S composite is shown in Fig. 1.

2.4. Material characterization

The microstructure and morphology of TiC–TiO_2/SWCNT/S composites and other control groups were characterized by scanning electron microscope (SEM), field emission scanning electron microscope (FE-SEM), scanning transmission electron microscopy (STEM) and selected area electron diffraction (SAED). The SEM was investigated by JEOL JSM-6510. The FE-SEM was performed with S-4700 type manufactured by HITACHI. The TEM was carried out by FEI Tecnai G2 F20 with STEM and SAED function. Powder X-ray diffraction (XRD) patterns of these composites were collected on an X-ray diffractometer (BRUKER D8 ADVANCE) from 10° to 80° with Cu Kα radiation. Raman spectroscopy was performed on a HORIBA XploRA system with a 532 nm laser. Thermogravimetric analysis (TGA, NETZSCH STA 449 F3) was performed from 28 to 500 °C at a heating rate of 10 °C per minute in N_2 atmosphere to determine the content of elemental sulfur. X-ray photoelectron spectroscopy (XPS, ESCALAB 250Xi, Thermo scientific) was used to characterize surface functional groups and chemical bonding states. The specific surface area and the pore size distribution of the product were tested by the Brunauer-Emmett-Teller (BET; 3H–2000PS2) through recording N_2 adsorption-desorption isotherms at 77.3 K.

2.5. Electrochemical measurements

CR2032-type coin cells were assembled in a glove box (Vigor Sci-Lab) under Ar-filled atmosphere and used for electrochemical characterization. TiC–TiO_2/SWCNT/S composites were used as the cathode (13 mm) and lithium tablets were used as anode (14 mm),

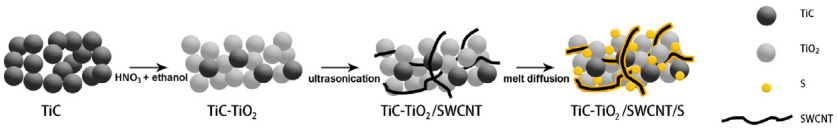

Fig. 1. Schematic diagram for preparing TiC—TiO_2/SWCNT/S composite.

which were separated by the Celgard 2400 separator (18 mm). The electrolyte was lithium bis (trifluoromethanesulfonyl) imide (1.0 M) dissolved in a mixture of lithium salt (LiTFSI) in dioxolane (DOL) and dimethoxyethane (DME) (1:1 by volume) with a 1.0 wt% $LiNO_3$ additive. To prepare the working electrode, a slurry was obtained by mixing and stirring the composite, conductive agent and binder: namely as-prepared TiC—TiO_2/SWCNT/S composite, super P (TIMCAL, Switzerland) and polyvinyldifluoride (PVDF, ARKEMA, Paris French) with the mass ratio of 8:1:1 in *N*-methyl-2-pyrrolidone (NMP, Aladdin, Shanghai China), respectively. The slurry is coated to the current collector (aluminum foil) by using a coating machine and vacuum dried for 12 h at 60 °C. The electrolyte amount is around 40 μl/mg sulfur and the sulfur loading ranges from 0.5 to 1 mg/cm^2.

Cyclic voltammetry (CV) was conducted at a scan rate of 0.1 $mV \cdot s^{-1}$ in a voltage range of 1.7—2.8 V and electrochemical impedance spectroscopy (EIS) was used in the frequency ranging from 5 mHz to 100 kHz with Autolab PGSTAT302 N electrochemical workstation. Galvanostatic charge/discharge tests were performed in the potential range of 1.7—2.8 V at 22 °C by using a Neware CT-4008 battery-testing instrument.

3. Results and discussion

3.1. Microstructure and morphology characterizations

To investigate the microstructures and morphologies of the modified cathodes, SEM and TEM images of different materials are conducted. Fig. S1a presents the low magnification SEM image of TiC—TiO_2/SWCNT/S 10 composite, which offers a large field of view of this composite. The corresponding EDS elemental mapping images of C, O, S and Ti in this large view are shown in Figs. S1b—e. It is clear that all the elements are dispersed well in the composite, demonstrating the uniform distribution of sulfur, SWCNT and TiC—TiO_2 in the composite. High-resolution FE-SEM and TEM images are further used to characterize the composite. Fig. 2a and Fig. S3a are the as-purchased TiC particles. After growing TiO_2 to form TiC—TiO_2, the surface becomes more rounded shape and most areas of the surface develop a porous structure (see Fig.2b and Fig. S3c). When the melted sulfur process is carried out, these TiC—TiO_2 particles are aggregated and inter-linked by a large amount of sulfur particles (Fig. 2c). In Fig. 2d, it is seen that a few batches of SWCNT are intertwined to the particles and the TiC—TiO_2/SWCNT/S 10 composite is formed. It is interesting that the addition of these SWCNTs preventing a full coating of non-conductive sulfur, thus enhances the dispersion of TiC—TiO_2/S particles and a high conductive network is built to improve the performance of batteries, and this structure is also beneficial to high utilization of sulfur. Actually SWCNT was reported in favor of forming a flexible and free-standing structure [16,36], so it is expected SWCNT would make the composite more robust and may overcome volume expansion of sulfur by this intertwine structure.

For the local details, TEM and STEM EDS mapping images are obtained. As seen in Fig. S2a, for TiC—TiO_2/S composites, the size of TiC—TiO_2 particles is range from 50 to 100 nm. Attractively, all these particles are wrapped with a thin sulfur layer as confirmed by an

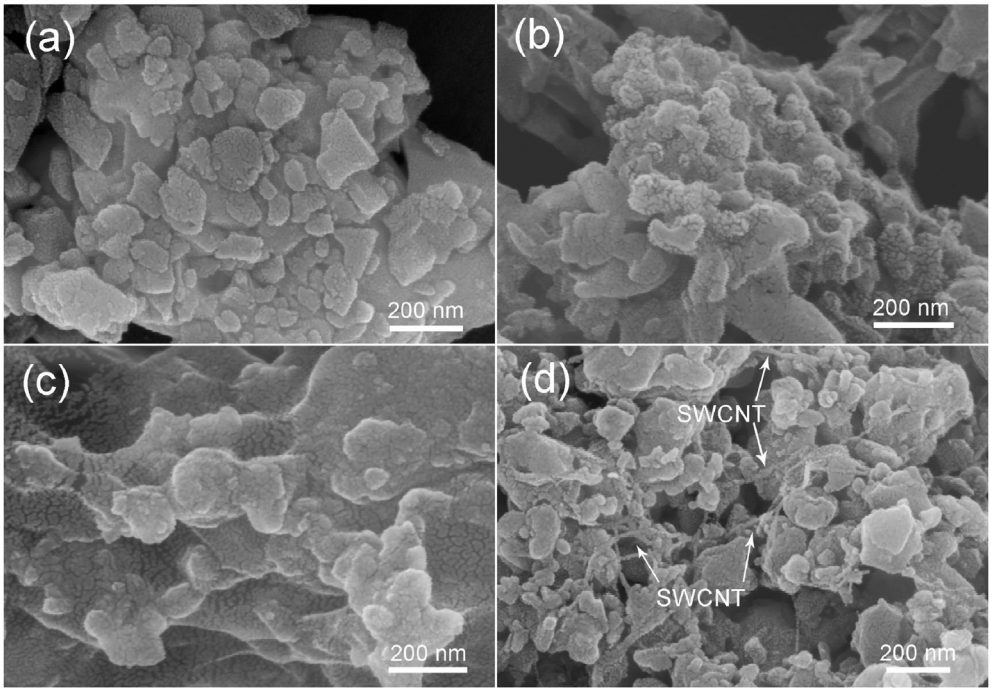

Fig. 2. FE-SEM images of (a) TiC, (b) TiC—TiO_2, (c) TiC—TiO_2/S and (d) TiC—TiO_2/SWCNT/S 10.

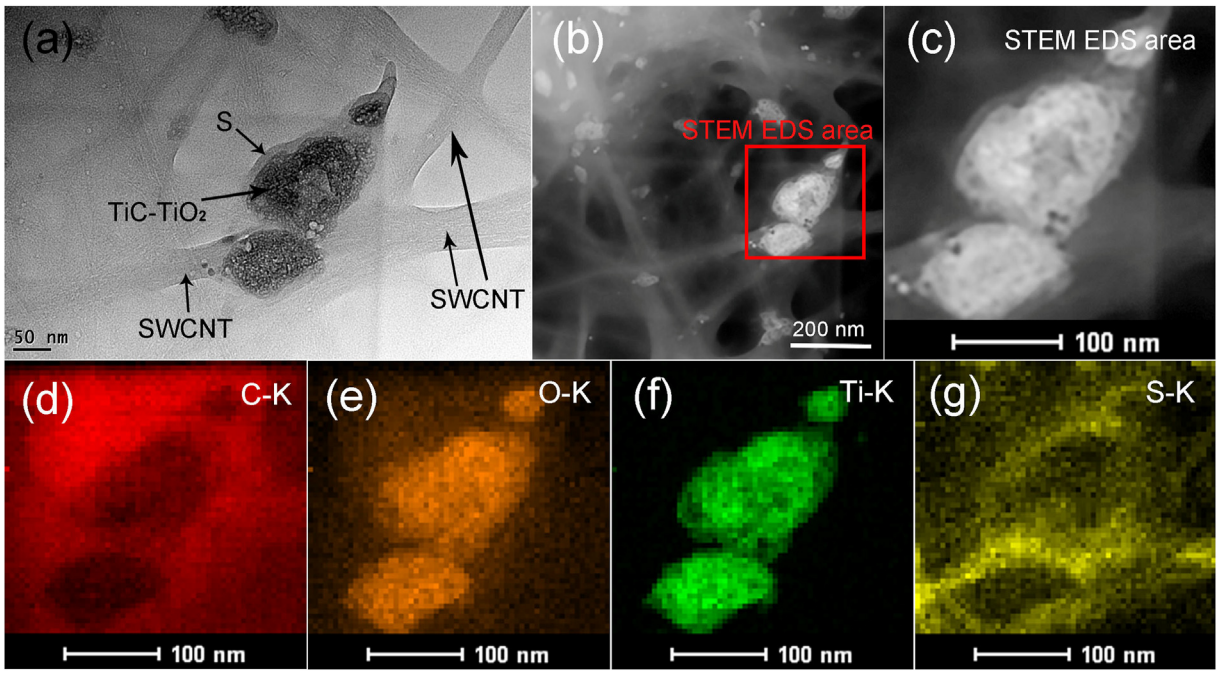

Fig. 3. (a) TEM image of TiC–TiO_2/SWCNT/S 10 composite; (b) STEM image with STEM EDS mapping area and (c) The enlarged view of marked area in (b); STEM EDS elemental mapping of (d) C, (e) O, (f) Ti, (g) S.

evidence from the STEM EDS sulfur elemental mapping of Fig. S2g. A uniform distribution in the composite is also observed from other elemental mapping images of C, O, Ti shown in Figs. S2d–f.

Fig. 3a shows the TEM images of TiC–TiO_2/SWCNT/S 10 composite. Compared to Fig. S2, the original TiC–TiO_2 particles with wrapped sulfur layer remain unchanged. The added SWCNTs serves as a network to link the TiC–TiO_2 particles. Moreover, there are some sulfur nanoparticles growing on the SWCNT surface [37,38], which is supported by Fig. 3g. Similarly, as shown in the STEM image (Fig. 3b and c) and STEM EDS mapping results (Fig. 3d–g), all the elements also distribute uniformly in the composite. Noticeably, the content of carbon is concentrated around the TiC–TiO_2/S particles due to the SWCNT is surrounding them (Fig. 3d) while the distribution of titanium has a clear boundary (Fig. 3f). In general, it is clear that SWCNTs intertwine the TiC–TiO_2/S tightly, which may benefit for ready electrons transport among different materials.

Fig. 4a is the Raman spectra of purchased TiC and TiO_2 powders, which are served as the baselines to compare the as-prepared TiC–TiO_2 composite. Their characteristic peaks are showed as black line (TiC) and red line (TiO_2) respectively. In Fig. 4b, for the as-prepared TiC–TiO_2 composite there are 4 peaks located at 141.8, 384.5, 506.7, and 619.3 cm^{-1}. As the molecular percentage of TiC is 33% and thus TiO_2 is 67% in TiC–TiO_2 composite (Table S1) and the composite presents peaks belong to more abundant materials, all the peaks for TiC cannot be observed. At the same time, peaks of TiC–TiO_2 composite are close to the characteristic peaks of TiO_2 in Fig. 4a but with a slight shift, reflecting some remaining pristine TiC particles. In Fig. 4b, for the final product TiC–TiO_2/SWCNT/S 10, there are no visible TiC and TiO_2 characteristic peaks, only sulfur peaks and three extra peaks for SWCNT (D band at 1333.0 cm^{-1}, G band at 1586.8 cm^{-1} and 2D band at 2665.4 cm^{-1}). The observation here is consistent that SWCNT is well-known for its distinct and intense Raman characteristic peaks even for a very small content [38–40]. Sulfur is dominant here because it takes nearly three quarters mass ratio in the composite. Moreover, as shown previously in the TEM image, the TiC–TiO_2 particles are typically enclosed by a large amount of sulfur. Although TiC has some chemisorption towards polysulfides [24], polysulfides mainly are adsorbed by surface oxidized TiO_2 in TiC–TiO_2.

Fig. 4c compares the XRD patterns of four different materials. Specifically, the green line is the diffraction peaks of purchased TiC. For the red line, three new weaker peaks located at 25.0°, 47.9° and 62.7° correspond to the crystal planes (101), (200) and (118) of TiO_2 [41]. The TiC–TiO_2/S composite mainly shows the diffraction peaks from sulfur such as (113), (222) and (026) because of the high content of sulfur, while all the peaks are weaker in the TiC–TiO_2/SWCNT/S 10 composite due to the addition of a small amount of SWCNT with broad peaks and the formation of smaller nano sulfur particles according to the BET results (see Fig. 6b) [38,42].

To determine the chemical composition of the as-prepared materials, XPS analysis was carried out for these composites. Fig. 4d displays the wide scan of TiC–TiO_2/SWCNT 10 composite (TiC: SWCNT = 10:1, mass ratio) and three peaks are corresponding to C 1*s*, O 1*s* and Ti 2*p*. According to the peak areas, the atomic content of carbon, oxygen and titanium are calculated as 13.7, 59.1 and 27.2 at.%. According to the relationship of weight (m), molar mass (M) and molecular weight (n) in the composite (see Table S1), it can be calculated that the molecular percentage of TiC in TiC–TiO_2 composite is 33% or the molecular ratio of TiC and TiO_2 is around 1:2. For the TiC–TiO_2/S composite, it can be seen that the conductivity of this composite is insufficient in previous work, because the nonconductive TiO_2 occupies a large proportion, more conductive agent is needed in slurry but the capacity was unsatisfactory at large current density [43,44]. Similarly, in Fig. 7c-d, poor performance is observed in our work for TiC–TiO_2/S composite with less conductive agent. The peaks at 284.7 eV, 286.6 eV, 288.8 eV refer to the C–C, C–O bonds and carbonate species while the peak at 281.1 eV could be assigned to C–Ti bond (Fig. 4e) [45–47]. For Ti 2*p* peaks in Fig. 4f, two peaks located at 459.0 eV and 464.6 eV are assigned to the Ti^{4+} oxidation state in TiO_2, whereas an extremely weaker peak located at 454.5 eV might result from a relatively small quantity of Ti–C [33].

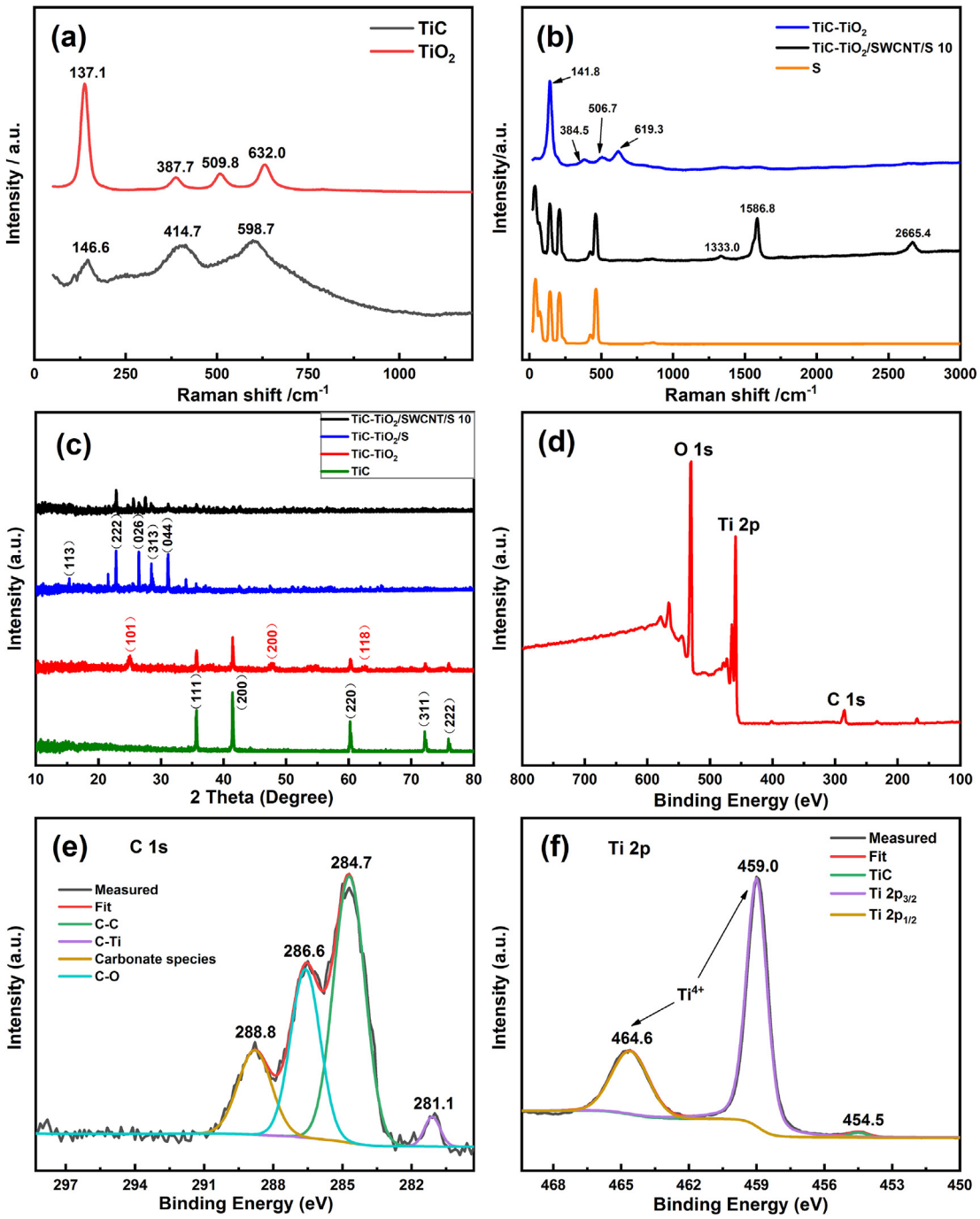

Fig. 4. Raman spectra of (a) purchased TiC and TiO_2; (b) three distinct materials; (c) XRD patterns of four different materials; XPS spectra of (d) TiC—TiO_2/SWCNT 10, its (e) C 1*s* and (f) Ti 2*p*.

The TGA curves of TiC—TiO_2/S, TiC—TiO_2/SWCNT/S 5 and TiC—TiO_2/SWCNT/S 10 composite are presented in Fig. 5. The sulfur contents of TiC—TiO_2/S, TiC—TiO_2/SWCNT/S 5 and TiC—TiO_2/SWCNT/S 10 composite are 74.3 wt%, 72.0 wt% and 70.4 wt% respectively. It is expected that sulfur content would further decrease with increasing the amount of SWCNT added. Therefore, it is important to balance the content of sulfur and the amount of SWCNT for a practical and cost-effective application. In our study, the slurry ratio is now 8:1:1 rather than the previous reported one 7:2:1 [33,34], which offers 10% more electrode material. However, from Fig. 5 it is only less than 4% sulfur in TiC—TiO_2/SWCNT/S 10 compared to that of TiC—TiO_2/S. Therefore, adding a small amount of SWCNT (10 wt% relative to TiC or around 2.01 wt% in TiC—TiO_2/SWCNT/S 10) has no negative effect to the energy density. On the contrary, there is 8% more active sulfur in electrode as a whole, making it attractive as high-performance Li—S batteries.

Fig. 6a shows the N_2 adsorption-desorption isotherms of TiC—TiO_2/SWCNT/S 10 composite. In previous work, the pore size distribution for TiC—TiO_2 is at the range of 2—10 nm with 158.99 $m^2 \cdot g^{-1}$ large specific surface area. On the contrary, TiC—TiO_2/S just has 8.24 $m^2\ g^{-1}$ low specific surface area and all the pores are larger than 5 nm because TiC—TiO_2 is almost filled with

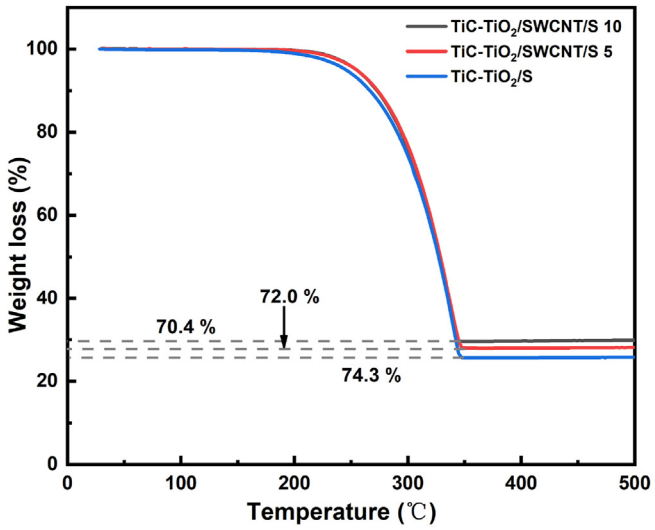

Fig. 5. TGA curves of TiC–TiO_2/S, TiC–TiO_2/SWCNT/S 5 and TiC–TiO_2/SWCNT/S 10 composites.

sulfur in TiC–TiO_2/S [33]. In our work, the situation of the TiC–TiO_2/S composite is similar to previous work [33] and it can be calculated that the specific surface area of TiC–TiO_2/SWCNT/S 10 composite is 12.08 $m^2 \cdot g^{-1}$, which is slightly higher than TiC–TiO_2/S composite, because of the addition of a small amount of SWCNT. Meanwhile, the formation of smaller nano sulfur particles contributes to this increase of the specific surface area. As a result, it appears a number of 2–5 nm pores again in TiC–TiO_2/SWCNT/S 10 and the average pore size is calculated to be 9.8 nm.

3.2. Electrochemical performance of batteries

The charge-discharge profiles in Fig. 7a show two discharge plateaus and one charge plateau during the process for all the composites. For TiC–TiO_2/SWCNT/S 10 composite, its discharge platforms appear at about 2.35 V and 2.10 V, corresponding to the reduction peaks of the CV curves in Fig. 8c. All the TiC–TiO_2/SWCNT/S cathodes display similar shape for the first cycle with less polarization and higher sulfur utilization, since those composites with SWCNT have good conductivity. Moreover, the intertwined networks formed by SWCNT can facilitate the reaction to polysulfides and further reaction of Li_2S_2 and Li_2S by offering effective electron tunnels and decreasing charge transfer resistance (verified in Fig. 9). However, the profile of TiC–TiO_2/S cathode has a large extent polarization (its discharge platforms appear at about 2.30 V and 2.05 V) as charge transfer resistance is higher without the connection of SWCNT. For the charge platform, different cathodes show a little difference and most of them appear at around 2.25 V.

As observed in Fig. 7b, the discharge specific capacities were obtained during cycling for the batteries of five different materials at 0.1 C. A significant high initial capacity of 1324.2 $mAh \cdot g^{-1}$ is delivered by the cell with TiC–TiO_2/SWCNT/S 10 cathode. The capacity maintains at 817.0 $mAh \cdot g^{-1}$ after 100 cycles with a satisfactory retention of about 60% to the initial value because of the high utilization rate of sulfur in modified crosslinked structure, as well as TiO_2 with strong adsorption of polysulfides. The cell with TiC–TiO_2/SWCNT/S 15 presents a very similar performance while a slightly low capacity of 802.5 $mAh \cdot g^{-1}$ was observed after cycles. In comparison, the cell with TiC–TiO_2/S composite shows the capacity 1157.3 $mAh \cdot g^{-1}$ and 657.9 $mAh \cdot g^{-1}$ with the capacity retention of 57% under the same condition. For the simple TiC/S cathode, its capacity decays to just 534.6 $mAh \cdot g^{-1}$ after 100 cycles from the value of 1202.4 $mAh \cdot g^{-1}$ at the beginning due to poor adsorption of polysulfides without TiO_2. Clearly, capacity for the cells with the addition of SWCNT were markedly superior to the cells without SWCNT, meanwhile TiO_2 also plays an important role in the improved cycling capacity as its good adsorption of polysulfides.

Long cycle performance of these cathodes at large current density of 1 C is presented in Fig. 7c. For the initial cycle, both TiC–TiO_2/SWCNT/S 10 and TiC–TiO_2/SWCNT/S 15 display a relatively high capacity, with 850.7 $mAh \cdot g^{-1}$ and 857.3 $mAh \cdot g^{-1}$ at the first cycle, respectively. After charged and discharged for 500 cycles, the capacity is about 666.5 $mAh \cdot g^{-1}$ for TiC–TiO_2/SWCNT/S 10 with 77.7% retention rate, and the values of TiC–TiO_2/SWCNT/S 15 are close to TiC–TiO_2/SWCNT/S 10, while a slightly lower capacity (799.1 $mAh \cdot g^{-1}$ at first cycle) is seen in the blue line for the composite with only 5% SWCNT added. The excellent large current performance found from the SWCNT modified cathodes is explained by that a small amount addition of SWCNT can improve the conductivity of cathode to a great extent. However, our results also reveal that adding too much SWCNT in the composite might not have obvious positive effect on enhancing the conductivity. Although having a relatively slow decay rate, it only achieves 671.0 $mAh \cdot g^{-1}$ at first cycle for the TiC–TiO_2/S composite, which means the conductivity of TiC–TiO_2/S is insufficient and its conductivity is the lowest among all the composites On the contrary, for the initial several cycles the cell with TiC/S offers better capacity than the cell with TiC–TiO_2/S because the conductivity of TiC/S is higher. However, without metal oxide of TiO_2, the TiC/S cathode alone is lacking the effective adsorption of polysulfide, resulting in a fast decay during whole cycle process as agreed to the performance shown in Fig. 7b at 0.1 C.

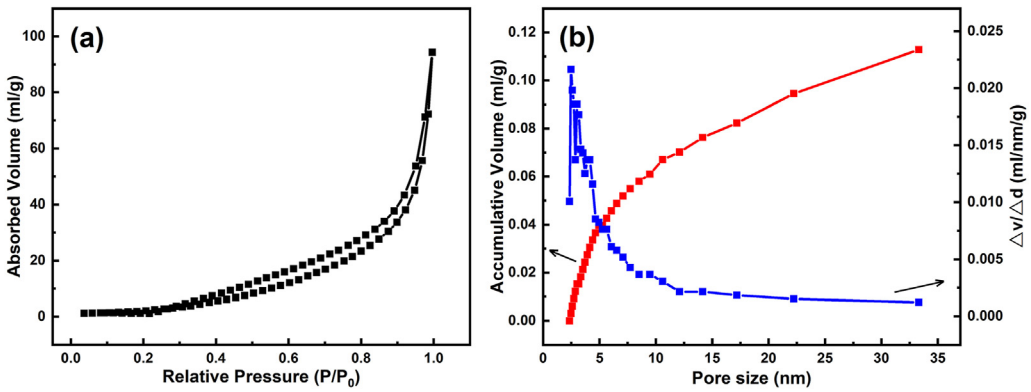

Fig. 6. (a) N_2 adsorption-desorption isotherm and (b) pore-size distribution curves of TiC–TiO_2/SWCNT 10.

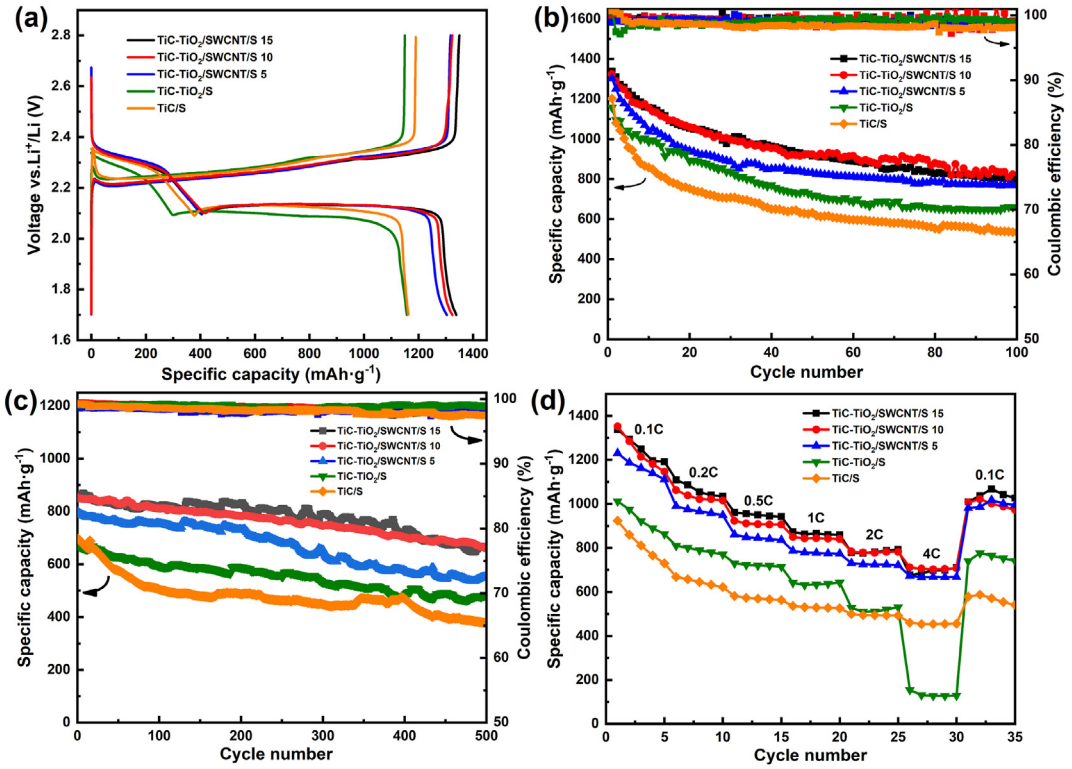

Fig. 7. (a) First charge-discharge curves; (b) Charge-discharge performance at 0.1 C, (c) Charge-discharge performance at 1 C large current density and (d) Rate performance from 0.1 C to 4 C of five different cathodes.

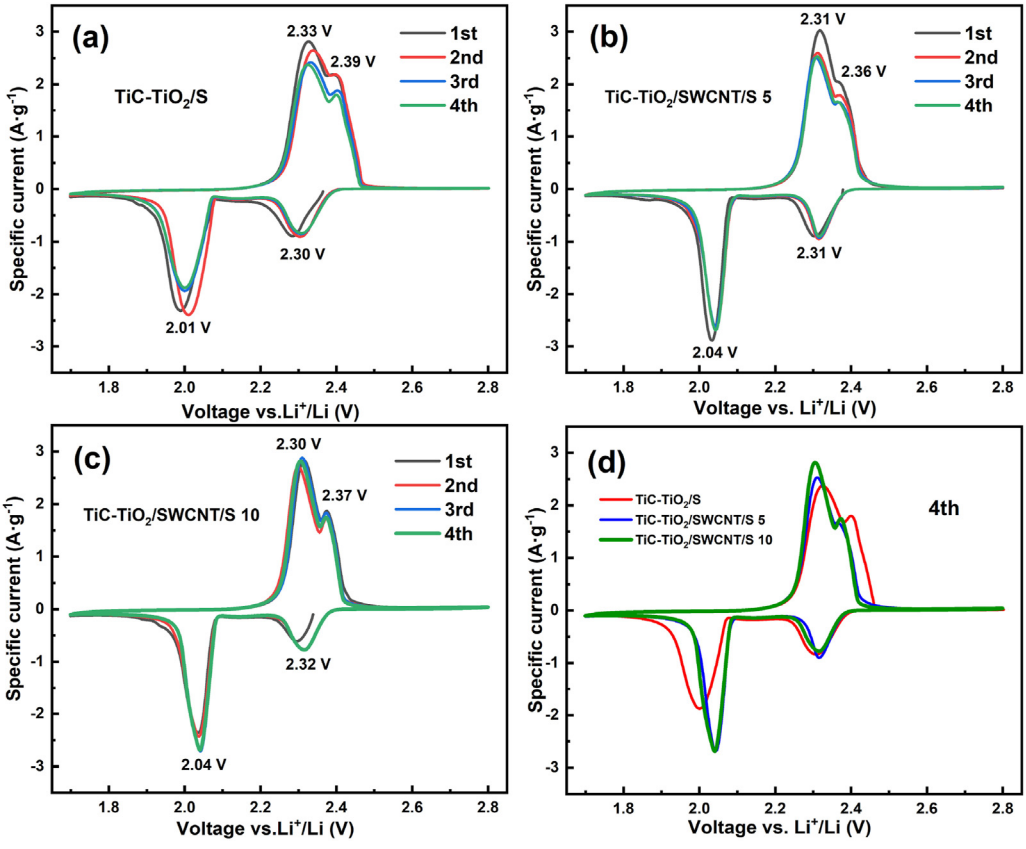

Fig. 8. CV plots for the first four cycles of (a) TiC–TiO_2/S, (b) TiC–TiO_2/SWCNT/S 5 and (c) TiC–TiO_2/SWCNT/S 10; (d) CV curves for the 4th cycle of different cathodes.

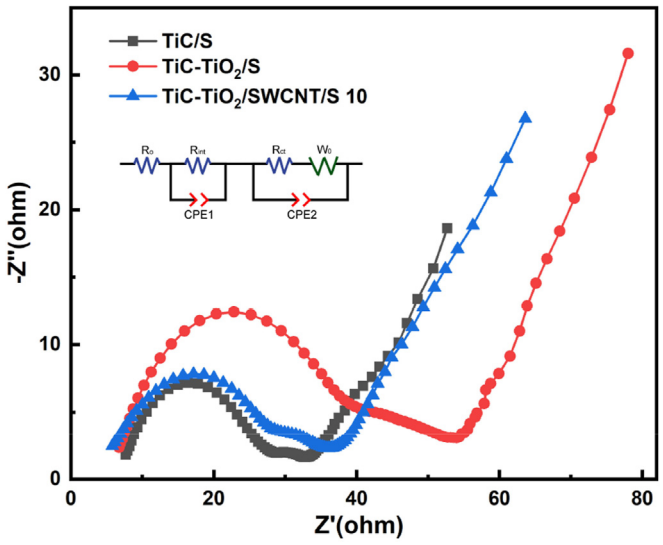

Fig. 9. EIS spectra of TiC—TiO_2/SWCNT/S 10, TiC—TiO_2/S and TiO_2/S cathodes (inset – corresponding equivalent circuit).

For the rate performance in Fig. 7d, the results are similar to the corresponding cycling performance as seen in Fig. 7b and c. The TiC—TiO_2/SWCNT/S 5 cell only dives to 673.2 mAh·g^{-1} at a high rate of 4 C and retains 981.2 mAh·g^{-1} when the current returns to 0.1 C. As expected, the cells with TiC—TiO_2/SWCNT/S 10 and TiC—TiO_2/SWCNT/S 15 cathodes present similar outstanding performance, but two curves can be still independently distinguished. The discharge capacity of TiO_2/SWCNT/S 10 reaches 711.2 mAh·g^{-1} at 4 C and recovers to 1006.9 mAh·g^{-1} when the current density resets to 0.1 C, which is significantly higher than 490 mAh·g^{-1} at 4 C reported in recent work [33]. This excellent rate performance and the recoverability are associated with the outstanding conductivity and the remarkably robust electrode structure after cycling at high current density (4 C). For the current density from 0.1, 0.2, 0.5, 1 C to 4 C and back to 0.1 C, the results of TiC—TiO_2/SWCNT/S 15 are slightly superior to TiC—TiO_2/SWCNT/S 10 in 0.1 C—1 C process, because adding SWCNT could improve the conductivity of the cathode and more efficient in accelerating the velocity of the redox reaction in the Li—S cell. However, this improvement is not that significant if considering the cost of adding extra 5% SWCNT, as well as it will decrease the energy density of the whole cell. Noticeably, the cell with TiC—TiO_2/S composite just achieves 155.3 mAh·g^{-1} at 4 C and its second discharge platform is below 1.8 V at 2 C current density on account of such low conductivity of TiC—TiO_2/S (Fig. S5b). To further understand the reason, Fig. S5 shows a comparison of charge and discharge profiles for rate performance of three electrodes. Due to the large polarization, TiC—TiO_2/S just shows one discharge platform when current is 4 C (Fig. S5b). On the contrast, although overall capacity of rate performance of TiC/S is lower, TiC/S with higher conductivity shows a smaller polarization and two full discharge platforms all the time in Fig. S5c. Therefore, TiC/S still remains 460.4 mAh·g^{-1} at 4 C large current density. Furthermore, compared with Fig. S5a and Fig. S5c, TiC—TiO_2/SWCNT/S 10 and TiC/S present almost the same degree of polarization, indicating that they have similar conductivity, verified in EIS results in Fig. 9. Obviously, both conductivities are markedly higher than TiC—TiO_2/S and thus the addition of SWCNT into TiC—TiO_2/S is essential for improving the performance of the Li—S batteries.

In addition, the electrochemical performances of TiO_2/S has been added for a comparison (Fig. S6). It is observed that for 1 C large current density performance, TiO_2/S presents a low specific capacity with just over 300 mAh·g^{-1}. Next, the capacity rises to about 600 mAh·g^{-1} because active sulfur and electrolyte mix uniform gradually, but it drops to a lower value after 500 cycles. For the rate performance, owing to the large resistance of TiO_2, TiO_2/S shows a very low capacity at 2 C and almost zero capacity when the current density increases to 4 C.

CV curves of three different batteries are shown in Fig. 8. For TiC—TiO_2/SWCNT/S 10, two reduction peaks are seen at 2.32 V and 2.04 V, corresponding to the reduction of elemental sulfur to high-order lithium polysulfides and the further reduction of high-order lithium polysulfides into Li_2S_2 and Li_2S during the discharge process. Two peaks at 2.33 V and 2.39 V refer to two oxidation process during charge process [48]. Starting point appears around 2.36 V at first cycle for all the batteries is associated with the self-discharge phenomenon of the cell after standing. If compared with Fig. 8a, b and 8c, it is clear that the redox peaks are gradually sharper and better overlapping feature for the initial several cycles with the addition of SWCNT. Among these three cathodes, the shape and the position of redox peaks of TiC—TiO_2/SWCNT/S 10 are the sharpest and the closest to the theoretical values. On the other hand, these peaks have almost no shifts on the following cycles for TiC—TiO_2/SWCNT/S 10, indicating the stable reaction pathway for the lithiation process. Meanwhile, with the addition SWCNT, the level of polarization gradually decreases and two oxidation peaks have become more pronounced. To compare more clearly, the CV curves for the 4th cycle presenting a relative stable condition of these three different batteries is illustrated in Fig. 8d. All these CV results are in a good agreement with charge-discharge curves shown in Fig. 7a.

EIS test can further demonstrate the impedance of cathodes. In Fig. 9, the semicircle in the high frequency region can be ascribed to the internal impedance of cathode (R_{int}), and a small arc of a semicircle locates in the medium frequency range refers to the charge-transfer resistance (R_{ct}) [33,49]. The short line in the low frequency region is generally named as Warburg resistance, denoted as W_0, which is attributed to the diffusion resistance of lithium ions within the cathode. CPE1 and CPE2 in the equivalent circuit represent the capacitive elements [50]. A corresponding equivalent circuit is inserted. It can be measured that the R_{int} of TiC—TiO_2/SWCNT/S 10 is 22.9 Ω, which is smaller than TiC—TiO_2/S (31.2 Ω) and bigger than TiC/S (16.4 Ω). Meanwhile, the R_{ct} of TiC—TiO_2/SWCNT/S 10 is 9.6 Ω, which is also lower than TiC—TiO_2/S (16.1 Ω) and even less than TiC/S (10.8 Ω). These phenomenon could be explained by surface oxidized TiO_2 leading to a relative high resistance for TiC—TiO_2/S. In addition, SWCNT can decrease resistance in TiC—TiO_2/SWCNT/S 10 by constructing a conductive network [38,43]. Moreover, a small amount of SWCNT interwined in TiC—TiO_2/SWCNT/S 10 composite can break non-conductive sulfur agglomeration in large areas, thus promoting material dispersion and decreasing charge-transfer resistance by providing numerous electron tunnels [51]. The structure can be seen in FE-SEM images in Fig. 2c and d and Fig.3a.

4. Conclusion

In summary, the TiC—TiO_2/SWCNT/S modified cathode for Li—S batteries was proposed and fabricated via a facile oxidation method. Compared with previous TiC—TiO_2/S cathode, TiC—TiO_2/SWCNT/S 10 with a small addition of SWCNT delivers 1324.2 mAh·g^{-1} specific capacity at first cycle and 817.0 mAh·g^{-1} after 100 cycles for 0.1 C, proving its higher conductivity and greater sulfur utilization. For rate performance, it shows 711.2 mAh·g^{-1} at 4 C and recovers to 1006.9 mAh·g^{-1} when current returns to 0.1 C. This cathode also reveals a good long cycling stability with 850.7 mAh·g^{-1} initial capacity and 77.7% retention rate after 500 cycles at

1 C large current density. Another attractive element for this study is that only a small amount of SWCNT (10 wt% relative to TiC in this case) is needed to enhance the conductivity of whole composite to a large extent. The overall cycling, rate performance and long cycling stability remain almost identical for adding 10% or 15% of SWCNT, indicating 10 wt% SWCNT is sufficient to offer good electrons transferring channels. Our results highlight that this strategy is efficient and low-cost to obtain high performance batteries, which has great potential to be applied in large-scale commercial applications.

CRediT authorship contribution statement

Xianwei Geng: Conceptualization, Methodology, Formal analysis, Investigation, Writing - original draft, Writing - review & editing. **Ruowei Yi:** Validation, Investigation. **Xiangfei Lin:** Validation. **Chenguang Liu:** Software. **Yi Sun:** Validation. **Yingchao Zhao:** Validation. **Yinqing Li:** Resources. **Ivona Mitrovic:** Supervision. **Rui Liu:** Resources. **Li Yang:** Resources, Writing - review & editing, Supervision, Project administration. **Cezhou Zhao:** Resources, Writing - review & editing, Supervision, Project administration.

Declaration of competing interest

The authors declare that they have no known competing financial interests or personal relationships that could have appeared to influence the work reported in this paper.

Acknowledgment

This work was supported by the National Natural Science Foundation of China (NSFC Grants 21750110441), State Key Laboratory of Materials Processing and Die & Mould Technology, Huazhong University of Science and Technology (P2019-019), Suzhou Industrial Park Initiative Platform Development for Suzhou Municipal Key Lab for New Energy Technology (RR0140), and Key Program Special Fund in XJTLU (KSF-A-04, KSF-E-28, and KSF-E-38).

Appendix A. Supplementary data

Supplementary data to this article can be found online at https://doi.org/10.1016/j.jallcom.2020.156793.

References

[1] P.G. Bruce, S.A. Freunberger, L.J. Hardwick, J.M. Tarascon, Li-O_2 and Li-S batteries with high energy storage, Nat. Mater. 11 (2011) 19–29.
[2] S. Zhang, K. Ueno, K. Dokko, M. Watanabe, Recent advances in electrolytes for lithium-sulfur batteries, Adv. Mater. 5 (2015), 1500117.
[3] Y.B. He, Z. Chang, S.C. Wu, H.S. Zhou, Effective strategies for long-cycle life lithium–sulfur batteries, J. Mater. Chem. 6 (2018) 6155–6182.
[4] Y. Liu, M.J. Yao, L.L. Zhang, Z.Q. Niu, Large-scale fabrication of reduced graphene oxide-sulfur composite films for flexible lithium-sulfur batteries, J. Energ. Chem. 38 (2019) 199–206.
[5] A. Fotouhi, D.J. Auger, K. Propp, S. Longo, M. Wild, A review on electric vehicle battery modelling: from Lithium-ion toward Lithium–Sulphur, Renew. Sustain. Energy Rev. 56 (2016) 1008–1021.
[6] Y.X. Yin, S. Xin, Y.G. Guo, L.J. Wan, Lithium-sulfur batteries: Electrochemistry, materials, and prospects, Angew. Chem. Int. Ed. 52 (2013) 13186–13200.
[7] T.B. Zeng, X.B. Hu, P.H. Ji, G.P. Zhou, Effects of sulfur carriers with different morphologies on performances of lithium-sulfur battery, Solid State Ionics 291 (2016) 47–68.
[8] A. Fu, C.Z. Wang, F. Pei, J.Q. Cui, X.L. Fang, N.F. Zheng, Recent advances in hollow porous carbon materials for lithium-sulfur batteries, Small 15 (2019), 1804786.
[9] Z.W. Seh, W.Y. Li, J.J. Cha, G.Y. Zheng, Y. Yang, M.T. McDowell, P.C. Hsu, Y. Cui, Sulphur-TiO_2 yolk-shell nanoarchitecture with internal void space for long-cycle lithium-sulphur batteries, Nat. Commun. 4 (2013) 1–6.
[10] K. Xi, D. He, C. Harris, Y.K. Wang, C. Lai, H.L. Li, P.R. Coxon, S.J. Ding, C. Wang, R.V. Kumar, Enhanced sulfur transformation by multifunctional FeS_2/FeS/S composites for high-volumetric capacity cathodes in lithium-sulfur batteries, Adv. Sci. 6 (2019), 1800815.
[11] H.S. Ryu, H.J. Ahn, K.W. Kim, J.H. Ahn, J.Y. Lee, E.J. Cairns, Self-discharge of lithium–sulfur cells using stainless-steel current-collectors, J. Power Sources 140 (2005) 365–369.
[12] H.S. Ryu, H.J. Ahn, K.W. Kim, J.H. Ahn, K.K. Cho, T.H. Nam, Self-discharge characteristics of lithium/sulfur batteries using TEGDME liquid electrolyte, Electrochim. Acta 52 (2006) 1563–1566.
[13] J. Liang, Z.H. Sun, F. Li, H.M. Cheng, Carbon materials for Li-S batteries: functional evolution and performance improvement, Energy Storage Mater 2 (2016) 76–106.
[14] Z.R. Tao, J.R. Xiao, Z.Y. Yang, H.W. Wang, Graphene/Sulfur@Graphene composite structure material for a lithium-sulfur battery cathode, J. Nnanomater. 2019 (2019) 1–10.
[15] D.D. Cheng, P.P. Wu, J.W. Wang, X.W. Tang, T. An, H. Zhou, D. Zhang, T.X. Fan, Synergetic pore structure optimization and nitrogen doping of 3D porous graphene for high performance lithium sulfur battery, Carbon 143 (2019) 869–877.
[16] R.P. Fang, K. Chen, L.C. Yin, Z.H. Sun, F. Li, H.M. Cheng, The regulating role of carbon nanotubes and graphene in lithium-ion and lithium-sulfur batteries, Adv. Mater. 31 (2019), 1800863.
[17] J.R. Xiao, H.Z. Wang, X.Y. Li, Z.Y. Wang, J.F. Ma, H. Zhao, N-doped carbon nanotubes as cathode material in Li-S batteries, J. Mater. Sci. Mater. Electron. 26 (2015) 7895–7900.
[18] J.R. He, Y.F. Chen, P.J. Li, F. Fu, Z. Wang, W.L. Zhang, Three-dimensional CNT graphene-sulfur hybrid sponges with high sulfur loading as superior-capacity cathode for lithium-sulfur batteries, J. Mater. Chem. 3 (2015) 18605–18610.
[19] K. Xi, B.G. Chen, H.L. Li, R.S. Xie, C.L. Gao, C. Zhang, R.V. Kumar, J. Robertson, Soluble polysulphide sorption using carbon nanotube forest for enhancing cycle performance in a lithium–sulphur battery, Nanomater. Energy 12 (2015) 538–546.
[20] Z. Li, Y. Huang, L. Yuan, Z. Hao, Y. Huang, Status and prospects in sulfur–carbon composites as cathode materials for rechargeable lithium–sulfur batteries, Carbon 92 (2015) 41–63.
[21] C.Y. Nan, Z. Lin, H.G. Liao, M.K. Song, Y.D. Li, E.J. Cairns, Durable carbon-coated Li_2S core-shell spheres for high performance lithium/sulfur cells, J. Am. Chem. Soc. 136 (2014) 4659–4663.
[22] J.W. Zhang, N. Yang, X.G. Yang, S.J. Li, J.M. Yao, Y.R. Cai, Hollow sulfur@graphene oxide core-shell composite for high-performance Li-S batteries, J. Alloys Compd. 650 (2015) 604–609.
[23] X. Song, T. Gao, S.Q. Wang, Y. Bao, G.P. Chen, L.X. Ding, H.H. Wang, Free-standing sulfur host based on titanium-dioxide-modified porous-carbon nanofibers for lithium-sulfur batteries, J. Power Sources 356 (2017) 172–180.
[24] H.J. Peng, G. Zhang, X. Chen, Z.W. Zhang, W.T. Xu, J.Q. Huang, Q. Zhang, Enhanced electrochemical kinetics on conductive polar mediators for lithium-sulfur batteries, Angew. Chem. 55 (2016) 12990–12995.
[25] M.S. Song, S.C. Han, H.S. Kim, J.H. Kim, K.T. Kim, Y.M. Kang, H.J. Ahn, S.X. Dou, J.Y. Leea, Effects of nanosized adsorbing material on electrochemical properties of sulfur cathodes for Li/S secondary batteries, J. Electrochem. Soc. 151 (2004) A791–A795.
[26] C.Y. Zha, F.L. Yang, J.J. Zhang, T.K. Zhang, S. Dong, H.Y. Chen, Promoting polysulfide redox reactions and improving electronic conductivity in lithium-sulfur batteries via hierarchical cathode materials of graphene-wrapped porous TiO_2 microspheres with exposed (001) facets, J. Mater. Chem. 6 (2018) 16574–16582.
[27] C. Y Zha, X.Q. Gu, D.H. Wu, H.Y. Chen, Interfacial active fluorine site induced electron transfer on TiO_2 (001) facets to enhance polysulfide redox reactions for better liquid Li_2S_6-based lithium-sulfur batteries, J. Mater. Chem. 7 (2019) 6431–6438.
[28] C.Y. Zha, D.H. Wu, T.K. Zhang, J.H. Wu, H.Y. Chen, A facile and effective sulfur loading method: Direct drop of liquid Li_2S_8 on carbon coated TiO_2 nanowire arrays as cathode towards commercializing lithium-sulfur battery, Energy Storage Mater 17 (2019) 118–125.
[29] C.Y. Zha, X.R. Zhu, J. Deng, Y. Zhou, Y.S. Li, J.M. Chen, P. Ding, Y.P. Hu, Y.F. Li, H.Y. Chen, Facet-tailoring five-coordinated Ti sites and structure-optimizing electron transfer in a bifunctional cathode with titanium nitride nanowire array to boost the performance of Li_2S_6-based lithium-sulfur batteries, Energy Storage Mater 26 (2020) 40–45.
[30] M.P. Yu, J.S. Ma, H.Q. Song, A.J. Wang, F.Y. Tian, Y.S. Wang, H. Qiu, R.M. Wang, Atomic layer deposited TiO_2 on a nitrogen-doped graphene/sulfur electrode for high performance lithium–sulfur batteries, Energy Environ. Sci. 9 (2016) 1495–1503.
[31] X. Liang, C.Y. Kwok, F. Lodi-Marzano, Q. Pang, M. Cuisinier, H. Huang, C.J. Hart, D. Houtarde, K. Kaup, H. Sommer, T. Brezesinski, J. Janek, L.F. Nazar, Tuning transition metal oxide-sulfur interactions for long life lithium sulfur batteries: the “Goldilocks” principle, Adv. Energy Mater. 6 (2016), 1501636.
[32] X.L. Ji, S. Evers, R. Black, L.F. Nazar, Stabilizing lithium-sulphur cathodes using polysulphide reservoirs, Nat. Commun. 2 (2011) 1–7.
[33] Z.Q. Cui, J. Yao, T. Mei, S.Y. Zhou, B.F. Hou, J. Li, J.H. Li, J.Y. Wang, J.W. Qian, X.B. Wang, Strong lithium polysulfides chemical trapping of TiC-TiO_2/S composite for long-cycle lithium-sulfur batteries, Electrochim. Acta 298 (2019) 43–51.
[34] X.S. Lang, Y.L. Zhao, K.D. Cai, L. Li, D.M. Chen, Q.G. Zhang, A facile synthesis of

stable TiO_2/TiC composite material as sulfur immobilizers for cathodes of lithium-sulfur batteries with excellent electrochemical performances, Energy Technol. 7 (2019), 1900543.
[35] D.E. Gu, Y. Lu, B.C. Yang, Y.D. Hu, Facile preparation of micro-mesoporous carbon-doped TiO_2 photocatalysts with anatase crystalline walls under template-free condition, Chem. Commun. 21 (2008) 2453–2455.
[36] C.H. Chang, S.H. Chung, A. Manthiram, Highly flexible, freestanding tandem sulfur cathodes for foldable Li-S batteries with a high areal capacity, Mater. Horiz. 4 (2017) 249–258.
[37] R.E. Carter, L. Oakes, N. Muralidharan, C.L. Pint, Isothermal sulfur condensation into carbon scaffolds: improved loading, performance, and scalability for lithium sulfur battery cathodes, J. Phys. Chem. C 121 (2017) 7718–7727.
[38] M.Q. Zhao, X.F. Liu, Q. Zhang, G.L. Tian, J.Q. Huang, W.C. Zhu, F. Wei, Graphene single-walled carbon nanotube hybrids one-step catalytic growth and applications for high-rate Li-S batteries, ACS Nano 6 (2012) 10759–10769.
[39] H.M. Heise, R. Kuckuk, A.K. Ojha, A. Srivastava, V. Srivastava, B.P. Asthana, Characterisation of carbonaceous materials using Raman spectroscopy: a comparison of carbon nanotube filters, single- and multi-walled nanotubes, graphitised porous carbon and graphite, J. Raman Spectrosc. 40 (2009) 344–353.
[40] M.Q. Zhao, Q. Zhang, J.Q. Huang, G.L. Tian, T.C. Chen, W.Z. Qian, F. Wei, Towards high purity graphene/single-walled carbon nanotube hybrids with improved electrochemical capacitive performance, Carbon 54 (2013) 403–411.
[41] K. Thamaphat, P. Limsuwan, B. Ngotawornchai, Phase characterization of TiO_2 powder by XRD and TEM, Nat. Sci. 42 (2008) 357–361.
[42] D.N. Futaba, K. Hata, T. Yamada, T. Hiraoka, Y. Hayamizu, Y. Kakudate, O. Tanaike, H. Hatori, M. Yumura, S. Iijima, Shape-engineerable and highly densely packed single-walled carbon nanotubes and their application as super-capacitor electrodes, Nat. Mater. 5 (2006) 987–994.
[43] Z.B. Xiao, Z. Yang, L. Wang, H.G. Nie, M.E. Zhong, Q.Q. Lai, X.J. Xu, L.J. Zhang, S.M. Huang, A lightweight TiO_2/graphene interlayer, applied as a highly effective polysulfide absorbent for fast, long-life lithium-sulfur batteries, Adv. Mater. 27 (2015) 2891–2898.
[44] Y.K. Wang, R.F. Zhang, J. Chen, H. Wu, S.Y. Lu, K. Wang, H.L. Li, C.J. Harris, K. Xi, R.V. Kumar, S.J. Ding, Enhancing catalytic activity of titanium oxide in lithium-sulfur batteries by band engineering, Adv. Energy Mater. 9 (2019), 1900953.
[45] A. Ignaszak, C.J. Song, W.M. Zhu, J.J. Zhang, A. Bauer, R. Baker, V. Neburchilov, S.Y. Ye, S. Campbell, Titanium carbide and its core-shelled derivative TiC@TiO_2 as catalyst supports for proton exchange membrane fuel cells, Electrochim. Acta 69 (2012) 397–405.
[46] X.Q. Guo, G.S. Zhang, H.Z. Cui, N. Wei, X.J. Song, J. Li, J. Tian, Porous TiB_2-TiC/TiO_2 heterostructures: synthesis and enhanced photocatalytic properties from nanosheets to sweetened rolls, Appl. Catal., B 217 (2017) 12–20.
[47] D.L. Shieh, S.J. Huang, Y.C. Lin, Y.S. Lin, J.L. Lin, T.F. Yeh, H. Teng, TiO_2 derived from TiC reaction in HNO_3: investigating the origin of textural change and enhanced visible-light absorption and applications in catalysis, Microporous Mesoporous Mater. 167 (2013) 237–244.
[48] D.W. Wang, Q.C. Zeng, G.M. Zhou, L.C. Yin, F. Li, H.M. Cheng, I.R. Gentle, G.Q.M. Lu, Carbon-sulfur composites for Li-S batteries: status and prospects, J. Mater. Chem. 1 (2013) 9382–9394.
[49] J.J. C, J. Xin, Q.J. She, C. Wang, Q. Zhang, M.S. Zheng, Q.F. Dong, The preparation of nano-sulfur/MWCNTs and its electrochemical performance, Electrochim. Acta 55 (2010) 8062–8066.
[50] N.A. Cañas, K. Hirose, B. Pascucci, N. Wagner, K.A. Friedrich, R. Hiesgen, Investigations of lithium-sulfur batteries using electrochemical impedance spectroscopy, Electrochim. Acta 97 (2013) 42–51.
[51] A. Anson-Casaos, C. Rubio-Munoz, J. Hernandez-Ferrer, A. Santidrian, A.M. Benito, W.K. Maser, Capacitive and charge transfer effects of single-walled carbon nanotubes in TiO_2 Electrodes, ChemPhysChem 20 (2019) 838–847.